Supplementary Materials

Optimizing diffusion kinetics of two-dimensional structures via nano-assembling towards rapid oxygen reduction electrocatalysis

Yang Yuan, Hongyan Wang, Ziwei Wen, Yueyue Wang, Qing Zhang*, Zhengyu Bai*

Collaborative Innovation Center of Henan Province for Green Manufacturing of Fine Chemicals, Key Laboratory of Green Chemical Media and Reactions, Ministry of Education, Henan Normal University, Xinxiang 453007, Henan, China.

***Correspondence to:** Prof. Zhengyu Bai, Dr. Qing Zhang, Collaborative Innovation Center of Henan Province for Green Manufacturing of Fine Chemicals, Key Laboratory of Green Chemical Media and Reactions, Ministry of Education, School of Chemistry and Chemical Engineering, Henan Normal University, No. 46 Jianshe Road, Xinxiang 453007, Henan, China. E-mail: baizhengyu@htu.edu.cn; zhangqing666@vip.163.com

1. MATERIALS AND CHARACTERIZATION

All the reagents are purchased commercially without further processing.

Physical and Chemical Characterization

Field emission scanning electron microscopy (FE-SEM; SU8010; Hitachi Ltd.) and transmission electron microscopy (TEM; JEM 2100 operating at 15 kV) were used to examine the morphology and structure of the samples. High-angle annular dark-field scanning TEM (HAADF-STEM) images are taken by a Hitachi aberration-corrected STEM HD-2700C. The composition of the sample was analyzed by X-ray photoelectron spectroscopy (XPS) on an ESCALAB250Xi instrument. Powder X-ray diffraction (XRD) was used to identify the crystal structure of the precursors and catalysts using an X'Pert3 Powder instrument. The pore structure was analyzed with N_2 adsorption-desorption measurements on a Brunauer–Emmett–Teller surface area analyzer (Quantachrome Instruments Quadra Sorb), and the pore-size distribution was obtained via the Barrett–Joyner–Halenda (BJH) model. Raman spectrum was recorded on a Raman spectrometer (LabRAM HR800). X-ray absorption fine structure (XAFS) spectra were collected on the 1W1B beamline of the Beijing Synchrotron Radiation Facility (BSRF, Beijing, China).

2. FIGURES AND TABLES

Supplementary Table 1. Structural parameters of the samples obtained by fitting the EXAFS data

Samples	Shell	CN	R (Å)	σ^2 (10^{-3} Å^2)	ΔE (eV)	R-Factor
Fe foil	Fe-Fe	8*	2.46	4.7	-4.0	0.002
	Fe-Fe	6*	2.84	4.8	-6.3	0.002
Fe-N-C NA	Fe-N	3.7	1.967	5.4	1.7	0.027

There are the average coordination number (CN), path distance (R), Debye-Waller factor (σ^2), threshold energy correction (ΔE), and the R-Factor of the fitting.

Supplementary Table 2. Adsorption edge positions of the samples

Samples	Pre-edge (eV)	Adsorption edge (eV)
Fe foil	-	7112
FeO	7111	7119
Fe-N-C NA	7111	7120
Fe_2O_3	7114	7124

It is derived from the energy corresponding to the first maximum of the first derivative of the XANES spectra of each sample after the pre-edge. The value of adsorption edge position increases with the elemental valence state.

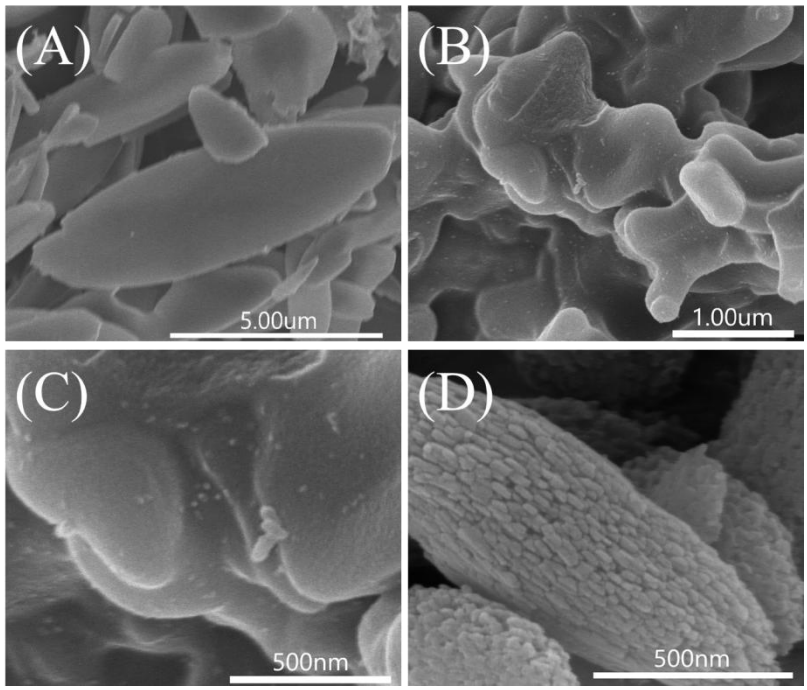

Supplementary Figure 1. SEM images of (A) ZIF-L bulk, (B and C) Fe-N-C bulk in different resolutions, and (D) Fe-N-C NA.

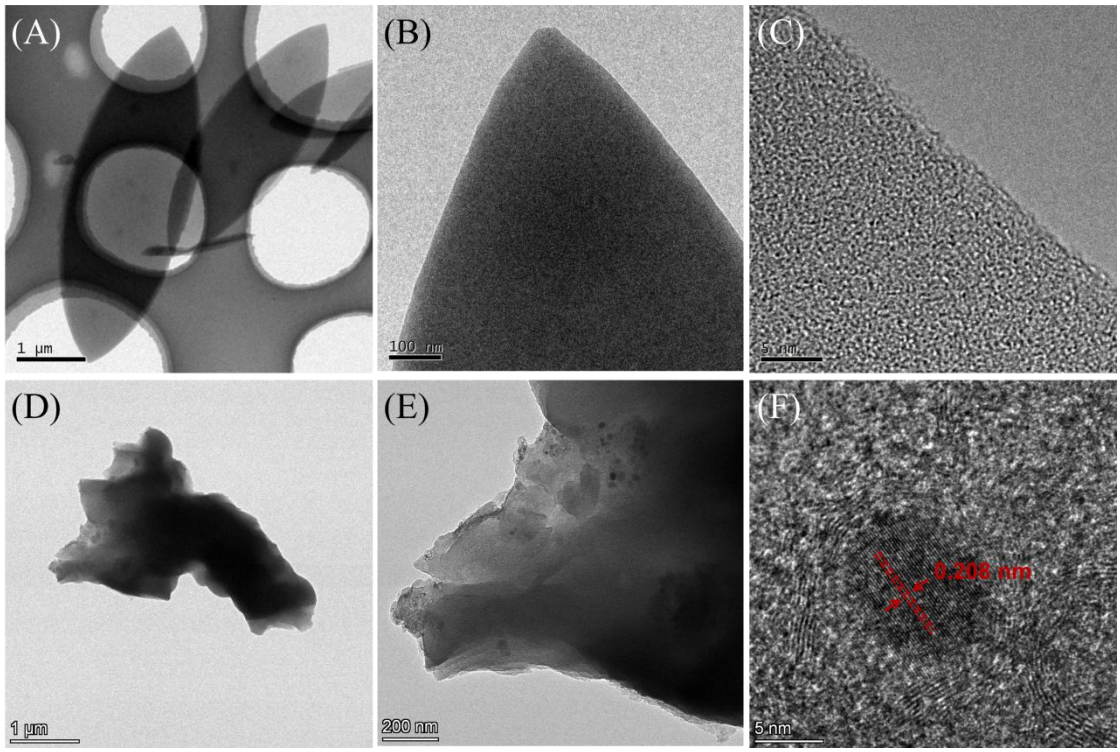

Supplementary Figure 2. TEM images of (A - C) ZIF-L bulk and (D and F) Fe-N-C bulk in different resolutions, respectively. The lattice spacing is measured to be 0.208 nm. It should be noted that the absence of corresponding diffraction signals in the PXRD pattern is possibly owing to the measurement precision of PXRD and the relative low content of the aggregates. Likewise, the absence of diffraction peak on the PXRD pattern lead to difficulties to determine the iron-based aggregate species accurately.

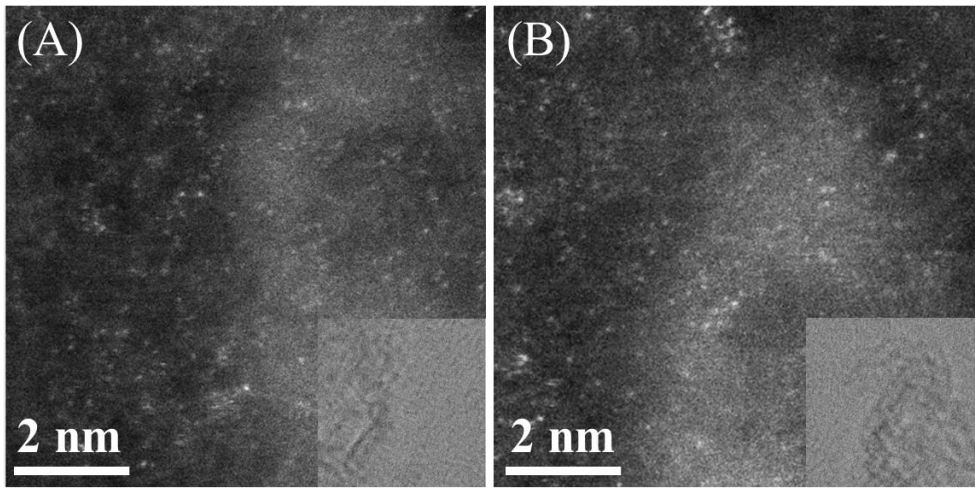

Supplementary Figure 3. AC-HR-HAADF-STEM and AC-HR-TEM (inset) images of Fe-N-C NA in randomly selected areas of (A) and (B).

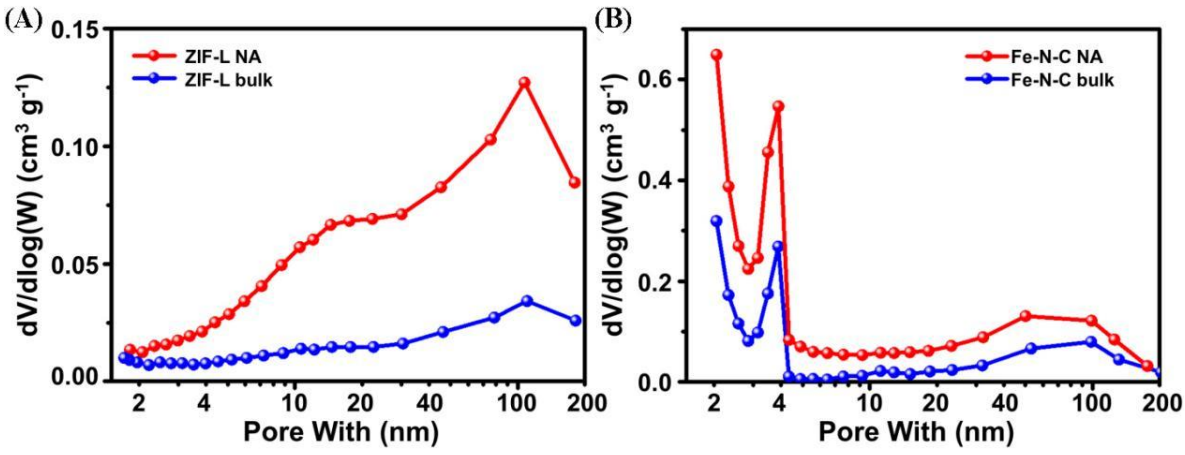

Supplementary Figure 4. Pore size distribution of ZIF-Ls and Fe-N-Cs calculated by BJH methods.

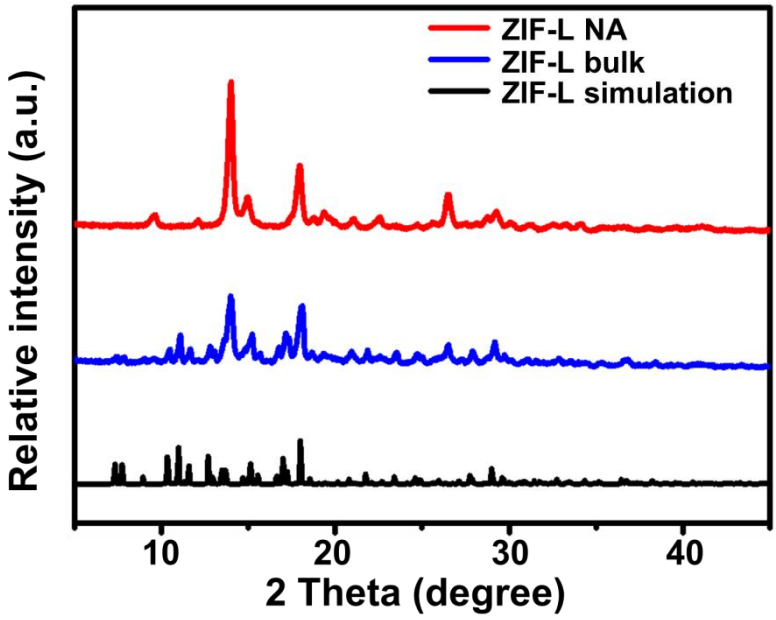

Supplementary Figure 5. PXRD pattern of the experimental and simulated ZIF-Ls.

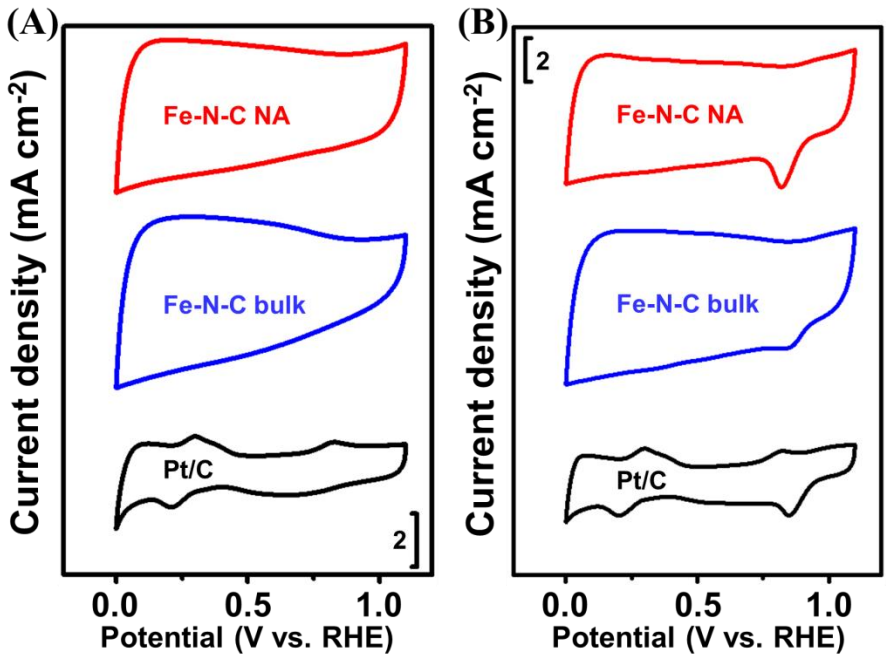

Supplementary Figure 6. CVs the catalysts under (A) N_2 and (B) O_2 saturated electrolyte.

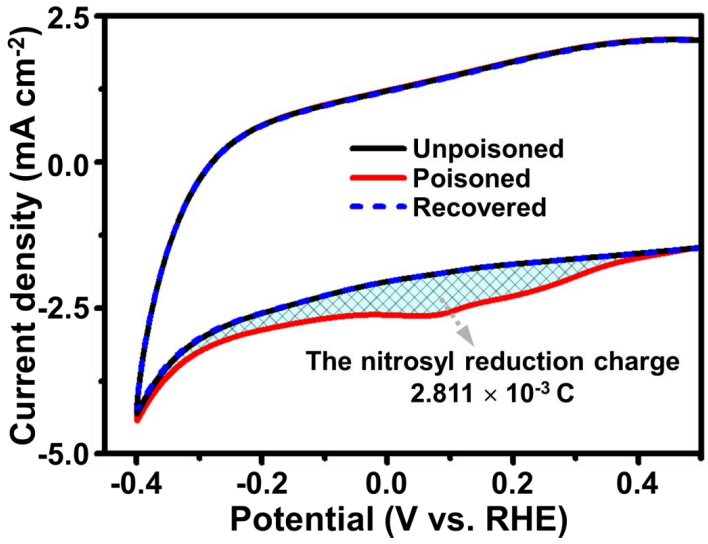

Supplementary Figure 7. CV curves in the nitrite reductive stripping region before, during and after nitrite adsorption.

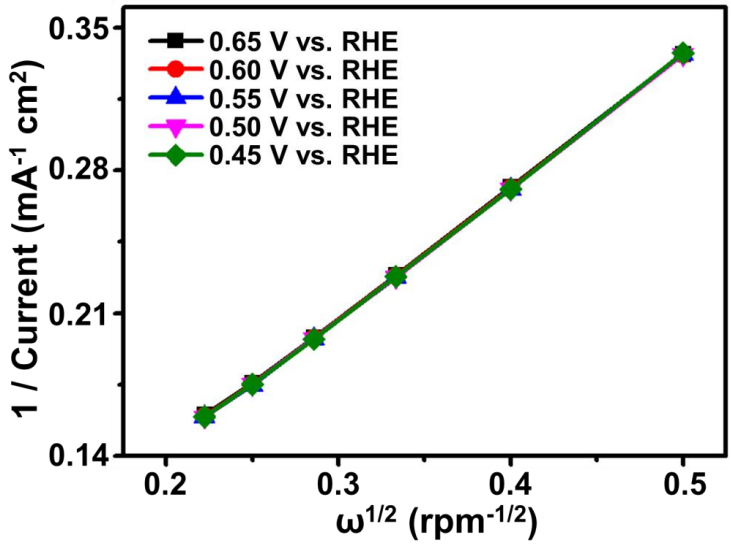

Supplementary Figure 8. K-L plots of Fe-N-C NA derived from the LSV curves.

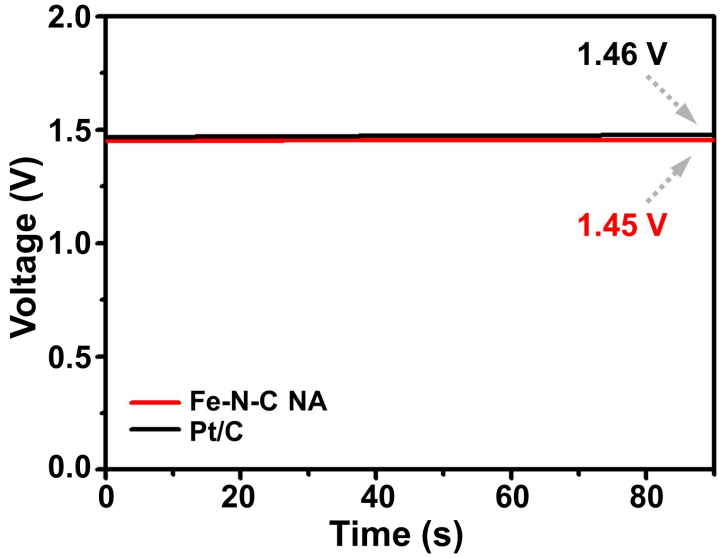

Supplementary Figure 9. Open circuit voltages of newly assembled ZABs driven by Fe-N-C NA and commercial Pt/C.

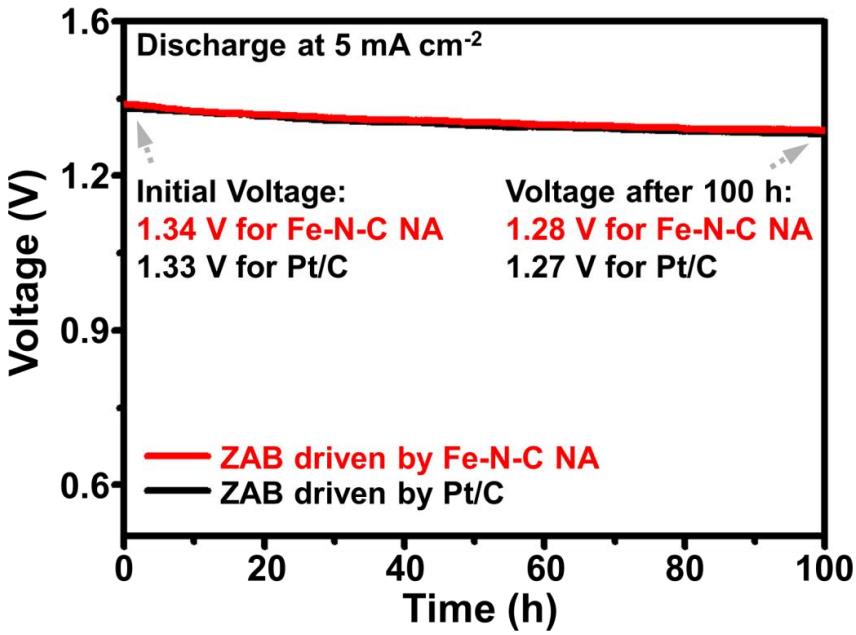

Supplementary Figure 10. Constant-current discharge measurements of assembled ZABs under 5 mA cm^{-2} and 100 sccm oxygen back flow to make the cathode withstand the long-term pressure of electrolyte without mechanical damages.

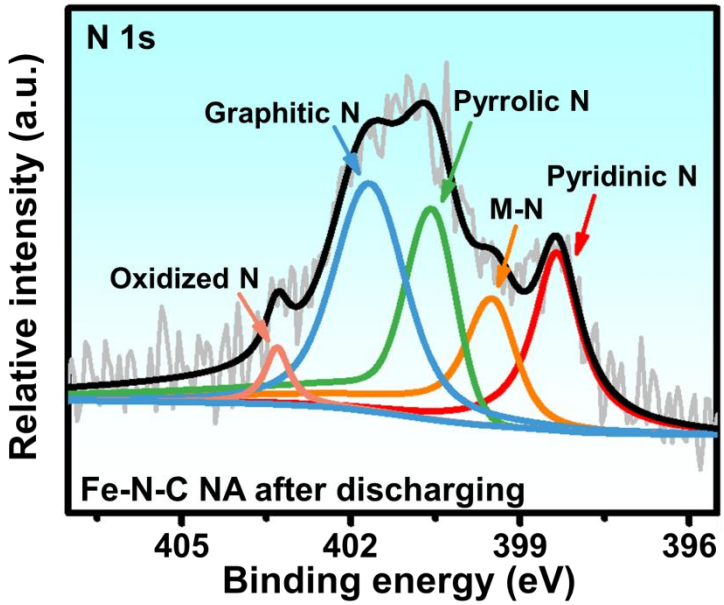

Supplementary Figure 11. XPS spectra for N 1s orbits of Fe-N-C NA after 100 h discharging under 5 mA cm^{-2}.

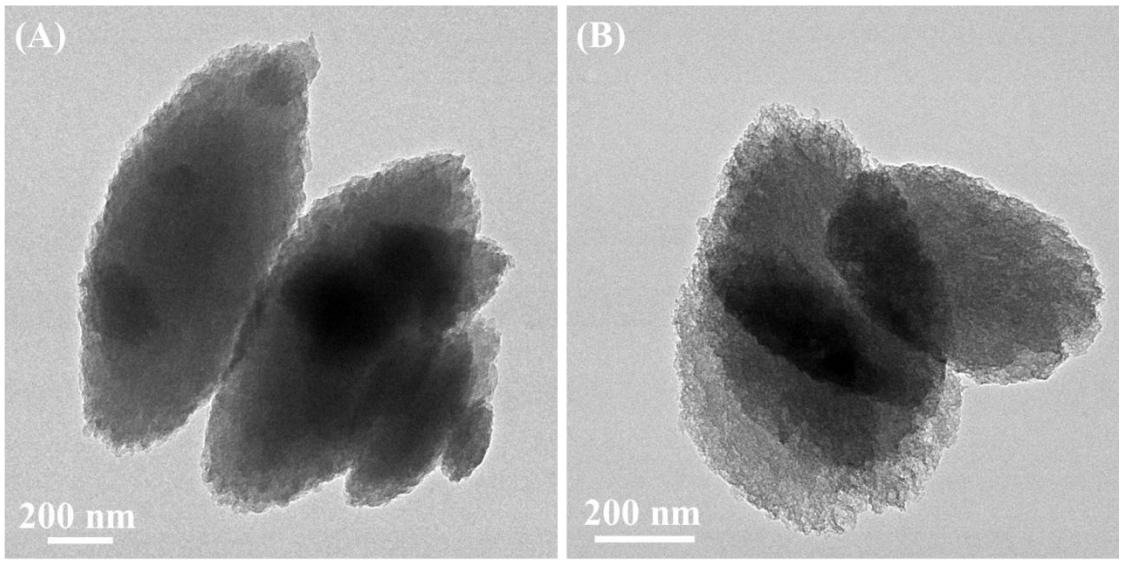

Supplementary Figure 12. HR TEM images of (A and B) the randomly selected Fe-N-C NA catalysts after the durability measurements of 100 h constant-current discharging under 5 mA cm^{-2}, which showed the morphology and porosity are maintained.